# Photocatalytic Events of CdSe Quantum Dots in Confined Media. Electrodic Behavior of Coupled Platinum Nanoparticles

**Clifton Harris and Prashant V. Kamat***

Radiation Laboratory and Department of Chemistry and Biochemistry, University of Notre Dame, Notre Dame, Indiana 46556, United States

**ABSTRACT** The electrodic behavior of platinum nanoparticles (2.8 nm diameter) and their role in influencing the photocatalytic behavior of CdSe quantum dots (3.4 nm diameter) has been evaluated by confining both nanoparticles together in heptane/dioctyl sulphosuccinate/water reverse micelles. The particles spontaneously couple together within the micelles *via* micellar exchange processes and thus facilitate experimental observation of electron transfer reactions inside the water pools. Electron transfer from CdSe to Pt is found to occur with a rate constant of $1.22 \times 10^9\ s^{-1}$. With the use of methyl viologen ($MV^{2+}$) as a probe molecule, the role of Pt in the photocatalytic process is established. Ultrafast oxidation of the photogenerated $MV^{+\bullet}$ radicals indicates that Pt acts as an electron sink, scavenging electrons from $MV^{+\bullet}$ with a rate constant of $3.1 \times 10^9\ s^{-1}$. The electron transfer between $MV^{+\bullet}$ and Pt, and a drastically lower yield of $MV^{+\bullet}$ under steady state irradiation, confirms the ability of Pt nanoparticles to discharge electrons quickly. The kinetic details of photoinduced processes in CdSe—Pt assemblies and the electrodic behavior of Pt nanoparticles provide important information for the development of light energy conversion devices.

**KEYWORDS:** photocatalysis · solar fuel · semiconductor quantum dots · interfacial electron transfer · metal nanoparticles

The coupling of semiconductor nanoparticles with noble metal cocatalysts has proven to be effective in photocatalytic reactions.[1−11] In particular, noble metal cocatalysts enhance the quantum yield of photoinduced electron transfer processes by (1) improving charge separation within the semiconductor particle, (2) discharging photogenerated electrons across the interface, and (3) providing a redox pathway with low overpotential. Earlier studies have shown that metal nanoparticles such as Pt promote hydrogen generation by intercepting photochemically reduced methyl viologen.[12−15] The present study is aimed at providing a better understanding of the physical and photoelectrochemical interactions between semiconductors and metals and the electrochemical properties of the metal cocatalyst.

The recent thrust in designing photocatalyst systems for solar fuel production[16−21] has further rejuvenated interest in semiconductor nanostructure-based hybrid assemblies. Of particular interest are the metal chalcogenides, which offer a significant advantage because of their tunable response to visible light.[22−26] While most of the photocatalytic studies focus on the net photoconversion efficiency, the understanding of various electron transfer steps at the fundamental level is still lacking. Early studies have explored timeframes with which photogenerated electrons and holes in a semiconductor nanoparticle are transferred across the interface.[27−36] Many of the interfacial charge transfer processes can be influenced by the presence of a metal cocatalyst. In particular, the ability of coupled metal nanoparticles to readily accept and shuttle electrons can be beneficially used to drive catalytic reactions. The storage/discharge capacity of metal nanoparticles has been probed through Fermi level equilibration between semiconductor−metal nanoparticles.[37−41] The important questions to answer are (1) how fast are electrons transferred from the excited semiconductor to the metal nanoparticles and (2) how does the electron equilibration between semiconductor and metal influence the overall energetic scheme and thus the charge transfer across the interface?

In the present study, the semiconductor−metal interactions were investigated at the nanoscale by confining CdSe quantum dots (QDs) and Pt nanoparticles in reverse micelles of heptane/dioctyl sulphosuccinate (AOT)/water. This methodology was similar to the one adopted previously to map the charge transfer processes between excited CdSe and methyl viologen.[42] Reverse micelles are stable, dynamic structures composed of a polar core

*Address correspondence to pkamat@nd.edu.

Received for review September 28, 2010 and accepted October 28, 2010.

**Published online November 11, 2010.**
**10.1021/nn102564x**

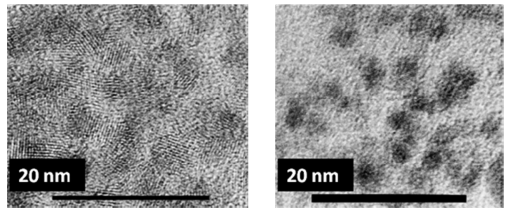


**Figure 1. High resolution TEM images of CdSe QDs (left) and Pt nanoparticles (right) prepared in reverse micelles.**

surrounded by surfactant molecules in a nonpolar bulk solvent. As inert "nano-cages", reverse micelles act both as templates for particle growth, and as confined chambers to carry out fast, efficient chemical reactions.[43] Reversed micelles have been used to synthesize size controlled metal nanoparticles[44−46] and quantum dots.[36,42,47−54] AOT is the preferred choice of surfactant because of its ability to form spherical droplets of controlled sizes.[36,55] The size of the water pool is directly related to the water−surfactant molar ratio, $w_o$.[56] Particle size, however, depends on an array of variables including precursor ratios, temperature, and pH. The synthesis of nanoparticles in reverse micelle provides a quick, low temperature synthetic approach. More importantly, it allows one to directly control the surrounding medium of the particles, and introduce other species into the pools, while retaining uncapped particle surfaces.

The dynamics of CdSe−Pt interactions in confined media, the kinetics and efficiency of electron transfer between CdSe and Pt, and the electrochemical behavior of Pt have now been investigated by using time-resolved transient spectroscopy to probe the photoinduced electron transfer events. An in-depth understanding of the charge transfer processes will enable the development of efficient photocatalyst systems for solar fuel generation.

## RESULTS AND DISCUSSION

**Characterization of Particles.** Figure 1 shows transmission electron microscopy (TEM) images of the CdSe and Pt nanoparticles prepared in reverse micelles. TEM provided the basis for obtaining the sizes of the CdSe and Pt nanoparticles. The particles were washed several times with excess water and centrifuged, resulting in a three-phase system. The water and excess surfactant were decanted. The washed nanoparticles were deposited on a carbon grid to record TEM images. The CdSe particles have an average size of 3.4 nm with 11% polydispersivity. The Pt particles have an average size of 2.8 nm with 16% polydispersivity. The diffraction pattern of the Pt nanoparticles exhibited a standard face-centered cubic structure. The absorption spectra of these nanoparticles in heptane/AOT/water reverse micellar suspension are shown in Figure 2.

**Coupling of CdSe and Pt Nanoparticles in Reverse Micelles.** To gain insight into the nature of the physical interactions between the particles, their arrangement among the

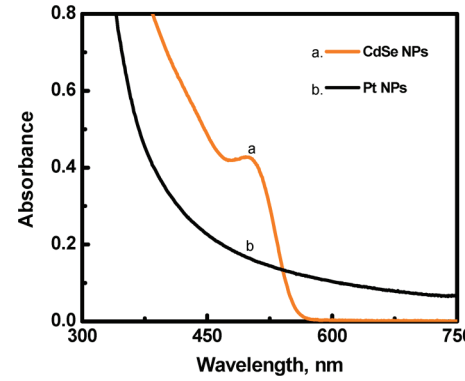


**Figure 2. Absorption spectra of 4 μm CdSe quantum dots and 4 μm Pt nanoparticles in heptane/AOT/water reverse micelles.**

micelles was considered. The distribution of solutes in reverse micelles is governed by Poisson statistics.[57] The probability of a micelle containing $n$ solutes can be expressed by

$$P(n) = \frac{\varphi^n e^{-\varphi}}{n!} \quad (1)$$

where $\varphi$ is the expected number of solutes per micelle. Therefore, the distribution of solutes is dependent on the size of the water pools. The radius of the pools is related to $w_o$ by[56]

$$\frac{r^3}{(r - L)^3} = 1 + \frac{V_2}{w_o V_1} \quad (2)$$

where $r$ is the water pool radius, $L$ is the length of an AOT molecule (15 Å), $V_2$ is the volume of an AOT molecule (825 Å$^3$), and $V_1$ is the volume of a water molecule (30 Å$^3$). The micelle concentration is inversely proportional to the square of the water pool radius by[36]

$$[M] = \frac{A[AOT]}{4\pi r_w^2} \quad (3)$$

where $A$ is the area of the AOT headgroup (0.55 nm$^2$). The distributions of the precursors, and the predicted distributions of the particles formed, are shown in the Supporting Information (SI-1). Micelles are dynamic structures which readily exchange contents *via* intermicellar collisions. Collisions lead to the formation of molecules, which agglomerate into small particles. These small particles undergo Ostwald ripening to form the particles shown in Figures 1 and 2.

The agglomeration numbers of the CdSe and Pt particles are 486 and 758, respectively. The particle concentrations can be obtained using the expression [p] = [C]/$n_a$, where [C] is the ion concentration of the limiting reactant (for CdSe, C is the concentration of $Se^{2-}$, and for Pt, C is the concentration of $PtCl_6^{2-}$), and $n_a$ is the agglomeration number. As a result of agglomeration, most of the micelles (~98%) are left empty following the completion of the particle growth. The maximum value of $P(n)$ occurs at $n = 0$ and decays rapidly

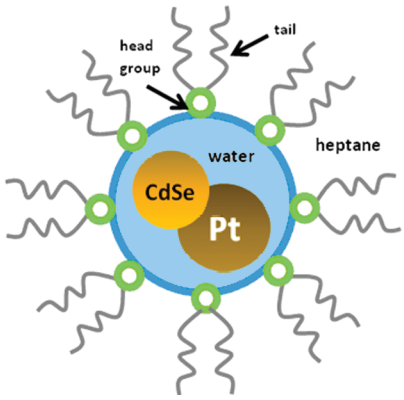


**Scheme 1. CdSe and Pt coupled in a heptane/AOT/water reverse micelle.**

as *n* approaches 1. Because [micelle] ≫ [particles], it may appear that the probability of a pool containing both CdSe and Pt particle based on Poisson statistics alone would be negligible. However, as will be seen in the forgoing discussion, the intermicellar exchange results in strong coupling of the CdSe and Pt nanoparticles within the same micelle. Therefore, particle distributions, unlike ion distributions, cannot be predicted using Poisson statistics due to such external factors as strong electrostatic attractions between the particles and thermodynamic stabilization of the occupied micelles.

**Ultrafast Electron Transfer at the CdSe Interface.** Electron scavenging by Pt nanoparticles at the CdSe surface reveals three key features with respect to the coupled system: (1) favorability of particle coupling in confined media, (2) kinetics of the electron transfer from CdSe to Pt, and (3) the electron injection efficiency across the CdSe−Pt interface. Femtosecond transient absorption measurements were conducted using 387 nm laser pulse excitation (fwhm 130 fs) to probe the photoinduced electron transfer processes between CdSe QDs and Pt nanoparticles. The CdSe−Pt composite micelles (Scheme 1) were obtained by mixing known aliquots of the two stock solutions. Figure 3A shows the time-resolved transient absorption spectra recorded at a few selected delay times. The bleaching seen at 510 nm corresponds to the depletion of the excitonic absorption band of CdSe. As shown in the previous study,[42,58−63] this bleaching arises from the charge separation following the laser pulse excitation of CdSe quantum dots. With increasing delay times, these charge carriers recombine and the observed bleaching recovers. Figure 3B shows the time-absorption profiles recorded at 510 nm, showing the bleaching recovery in the absence and in the presence of Pt nanoparticles. These Pt nanoparticles exhibit the distinct effect of enhancing the rate of bleaching recovery as the photogenerated electrons are transferred from excited CdSe into Pt nanoparticles. If we assume the increased recovery is due to the interparticle electron transfer, we can estimate the rate constant of electron transfer. A similar approach has been found to be useful in estimating electron transfer between excited CdSe and $TiO_2$ nanoparticles.[42,64,65]

The bleaching recovery traces in Figure 3B are multiexponential and can be analyzed using a triexponential expression eq 4, where the parameters $a_1$, $a_2$, and $a_3$ are the relative amplitudes of each lifetime component τ. The average lifetime, ⟨τ⟩, of a given process is calculated by eq 5, using the normalized components ($\mathbf{A}_i = a_i\tau_i/(\sum a_i\tau_i)$).[66]

$$\Delta A(t) = a_1 e^{(t/\tau 1)} + a_2 e^{(t/\tau 2)} + a_3 e^{(t/\tau 3)} \quad (4)$$

$$\langle\tau\rangle = [\sum(\mathbf{A}_i\tau_i^2)]/\sum(\mathbf{A}_i\tau_i) \quad (5)$$

The interparticle electron transfer is a static process, as the electron transfer processes in question occur on a much faster time scale than the estimated time of micellar exchange (>1 μs), and also because the particles are confined within the nanosized micelle cores. Thus, the ultrafast processes observed during the femtosecond transient absorption experiments are *not* diffusion limited and should therefore should be independent of acceptor concentration. The rate constant of the electron transfer process is defined as the reciprocal of the average lifetime. Since the bleaching recovery shown in trace a in Figure 3B is attributed to

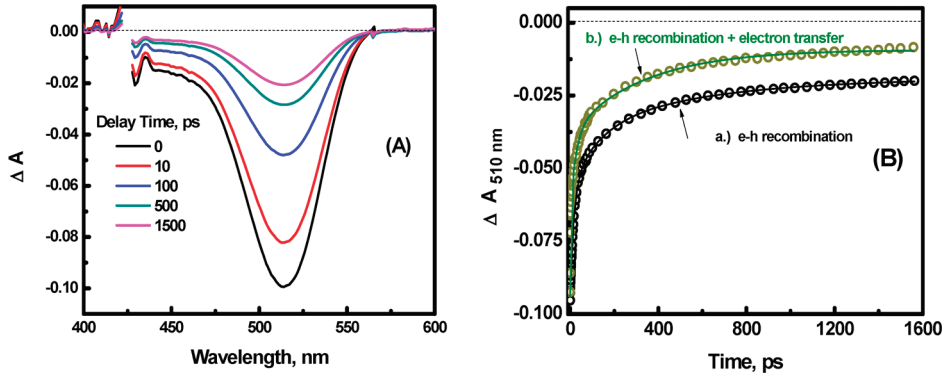


**Figure 3. (A) Transient absorption spectra of 4 μM CdSe in heptane−AOT−water reverse micelles recorded following 387 nm laser excitation at different delay times. (B) Time−absorption profiles showing the bleaching recovery of CdSe at 510 nm (a) in the absence and (b) in the presence of 4 μM Pt.**

electron−hole recombination processes, and trace b corresponds to the sum of the rates of recombination and electron transfer processes, we can estimate the rate of electron transfer from CdSe to Pt using

$$k_{et} = 1/\tau_{(CdSe+Pt)} - 1/\tau_{(CdSe)} \quad (6)$$

The corresponding rate constants derived from the traces are $1.80 \pm 0.16 \times 10^9$ s$^{-1}$ ($k_a$) and $3.02 \pm 0.11 \times 10^9$ s$^{-1}$ ($k_b$), respectively. The rate constant of electron transfer from excited CdSe into Pt was $k_{ET} = 1.22 \pm 0.19 \times 10^9$ s$^{-1}$. The high rate constant of the electron transfer reaffirms that the interactions between the CdSe and Pt nanoparticles are static. Additionally, we can also estimate the maximum attainable efficiency of electron transfer during the initial encounter from the rate constant of recovery of the CdSe and CdSe−Pt systems. From this analysis, it is determined that 40% of the electrons generated following the pulse excitation are scavenged by Pt nanoparticles.

**The Role of Pt in Mediating Electron Transfer.** In the previous section, we investigated the electron transfer between CdSe and Pt. The next step would be to see how Pt affects the electron transfer between CdSe and a probe molecule. There are several possible ways that Pt could influence the electron transfer process. For example, Pt could act as an electron shuttle, improving charge separation at the CdSe surface by quickly scavenging photogenerated electrons, then transferring those electrons to the probe molecule, hence, enhancing the efficiency of the reduction and the yield of the reduced probe species. Pt particles may also compete with probe molecules for photogenerated electrons at the CdSe interface or undergo charge equilibration with reduced probe molecules. Thus, the Pt particles would either store the electrons or quickly discharge the electrons into the medium (*e.g.*, to $H^+$ ions to produce hydrogen). The examples of photocatalytic production of water highlight the electron discharge capability of metal nanoparticles.

Methyl viologen ($MV^{2+}$) is an excellent probe for monitoring photoinduced electron transfer at the semiconductor interface due to its favorable redox potential, pH independence, and unique spectral characteristics. The $MV^{2+}$ cation readily undergoes 1-electron reduction ($E^0 = -0.445$ V *vs* NHE) to form the cationic radical, $MV^{+\bullet}$, which has a characteristic blue color ($\varepsilon = 13700$ M$^{-1}$ cm$^{-1}$ at 605 nm).[67] In addition, $MV^{+\bullet}$ is capable of transferring electrons to Pt nanoparticles, which in turn reduces surface adsorbed $H^+$ ions to produce hydrogen.[68] Thus, by monitoring the changes in the formation of the $MV^{+\bullet}$ radical with and without Pt, we should be able to establish the role of Pt in the photocatalytic system. The absorption spectra of the radical can be found in the Supporting Information (SI-4).

A known concentration of $MV^{2+}$ dispersed in heptane/AOT/water was mixed with CdSe and CdSe/Pt dispersions of reverse micelles. Care was taken to maintain equal $w_0$ values. The distribution of $MV^{2+}$ molecules among the micelles is described in the Supporting Information (SI-2). The high concentration of $MV^{2+}$ employed in our measurements ensured that $[MV^{2+}] \gg$ [CdSe] within the reverse micellar medium. At such concentrations, the CdSe and CdSe−Pt systems can readily interact with $MV^{2+}$ within the same micelle, as the surface of CdSe is saturated with $MV^{2+}$ (see Supporting Information SI-3). As previously stated, the interactions within micelles as established from femtosecond transient spectroscopy are static processes. Therefore, the kinetic data obtained from the transient absorption measurements exhibit first-order dependence. This observation differs from the second-order dependence observed for diffusion controlled interactions between $MV^{+\bullet}$ and Pt colloids in other systems.[12−15] Slower kinetic events (μs−ms time frame) corresponding to the back electron transfer were also observed in these studies.

Figure 4 panels A and B show the changes in absorbance *versus* delay time monitored at the excitonic peak of CdSe (510 nm) and at the absorption peak of the $MV^{+\bullet}$ radical (605 nm), following the excitation of the CdSe and CdSe/Pt systems. The panels on the right show a selected region with an expanded time scale to highlight the influence of Pt on the bleaching recovery and $MV^{+\bullet}$ formation. A flow cell was employed in these measurements to avoid interference from the $MV^{+\bullet}$ radical accumulation. The spectra recorded immediately after the 387 nm laser pulse excitation shows transient bleaching at the excitonic band. However, the spectra recorded after ~10 ps delay shows additional broad absorption in the 600 nm region. The appearance of the absorption band with a maximum at 605 nm confirms the photoinduced electron transfer to produce $MV^{+\bullet}$, and also shows that the electron transfer to $MV^{2+}$ from excited CdSe is an ultrafast event (see Supporting Information, SI-5).

The bleaching recovery of CdSe (trace c) is significantly faster when $MV^{2+}$ is present. As discussed in our previous study, such a fast recovery represents electron transfer to $MV^{2+}$ and is further supported by the appearance of the $MV^{+\bullet}$ radical with absorption in the 600 nm region. The rate constant of the exciton bleaching recovery of CdSe in the presence of $MV^{2+}$ is estimated to be $1.7 \pm 0.11 \times 10^{10}$ s$^{-1}$. The rate constant of electron transfer from CdSe to $MV^{2+}$ (trace c) is given by $k_{ET} = 1/\tau_{(CdSe+MV)} - 1/\tau_{(CdSe)}$, approximately $1.52 \times 10^{10}$ s$^{-1}$.

In the presence of both Pt and $MV^{2+}$ (trace d), the recovery of the bleaching is enhanced by an order of magnitude, yielding an electron transfer rate constant of $1.7 \pm 0.5 \times 10^{11}$ s$^{-1}$. In this case, $k_{(CdSe+MV+Pt)} \gg (k_{CdSe} + k_{CdSe+Pt} + k_{CdSe+MV})$, indicating a synergistic effect on the electron transfer rate when CdSe is coupled with both Pt and $MV^{2+}$. The exact reasons for this effect are

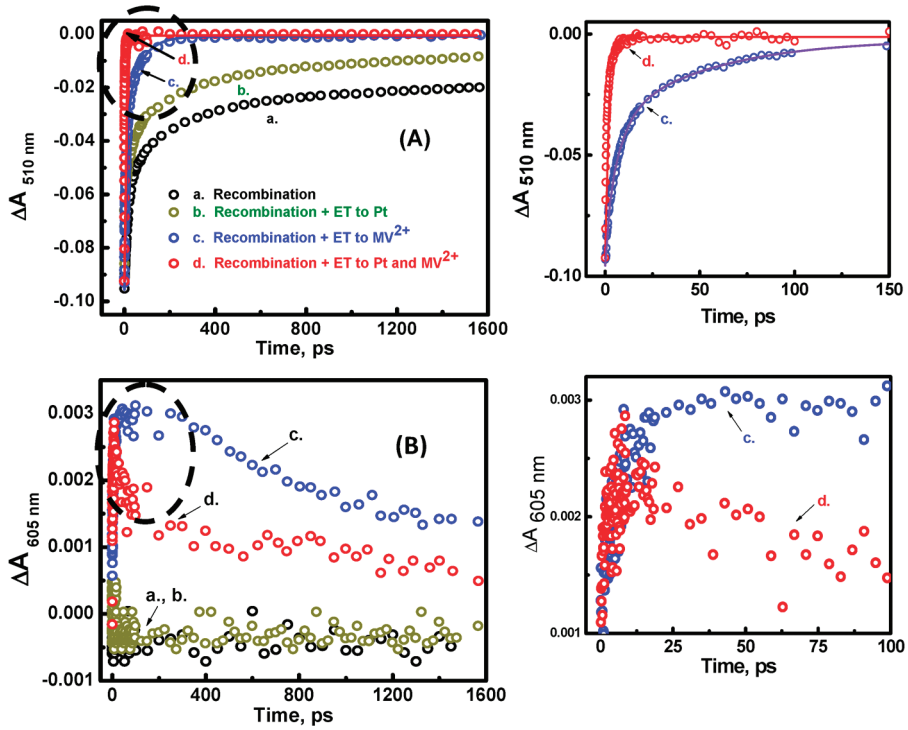


**Figure 4. Time absorption profiles monitored at (A) 510 nm (bleaching recovery of CdSe) and (B) 605 nm (formation and decay of $MV^{+\bullet}$) following 387 nm laser pulse excitation of 4 μM CdSe confined in a heptane/AOT/water reverse micelle: (a) CdSe alone; (b) CdSe + 4 μm Pt NP; (c) CdSe + 1 mM $MV^{2+}$; (d) CdSe + 1 mM $MV^{2+}$ + 4 μM Pt NP. The figure to the right is a magnified view of the circled region, which shows the evolution of ultrafast kinetic traces of panels c and d.**

unknown, but large enhancements in reaction rates inside of micelles have been previously observed for other systems.[42,69−73] Surfactant−water interface interactions, strong electric fields, and changes in the chemical properties of water under confined conditions are several unique attributes of reverse micelles which have long been suspected of influencing photochemical reactions.[74] Achieving fast electron transfer across the interface is an important criterion to maximize the efficiency of photoconversion.

An interesting difference in the transient absorption of $MV^{+\bullet}$ is seen as the transient absorption is probed at longer time scales (traces c and d in Figure 4B right panel). In the presence of Pt, the $MV^{+\bullet}$ exhibits a sharp decay within 100 ps. In the absence of Pt nanoparticles, the $MV^{+\bullet}$ remains stable during the same time period. The decay of the $MV^{+\bullet}$ absorbance indicates fast oxidation of $MV^{+\bullet}$ by Pt. These preliminary results suggest that Pt acts as an electron sink. We estimate the rate constant of electron transfer between $MV^{+\bullet}$ and Pt to be $3.1 \times 10^9\ s^{-1}$.

**Influence of Pt Nanoparticles on the Steady State Yield of $MV^{2+}$.** The steady state accumulation of $MV^{+\bullet}$ in the present experiments was monitored in the absence and presence of Pt. An Ocean Optics UV−vis spectrometer was employed to monitor the absorbance changes during visible light irradiation of CdSe suspensions containing (i) $MV^{2+}$, and (ii) $MV^{2+}$ and Pt. The absorbance values at 605 nm for each time interval were compiled and plotted *versus* time (Figure 5A,B) to probe the build-up of the $MV^{+\bullet}$ radical. The excitation source was a xenon lamp passed through a 450 ± 10 nm narrow band-pass filter. This configuration allowed selective excitation of CdSe. (The $MV^{+\bullet}$ radical does not absorb in this region, and the absorbance of Pt is minimal at the experimental concentrations.) Under these conditions, the Pt particles remain stabilized and we do not see any evidence for aggregation effects. Increasing the Pt concentration thus results in increased number of Pt particles within the micelle.

Reduction of $MV^{2+}$ proceeds following the excitation of CdSe, and the radical attains a steady state concentration in about 400 s in the absence of Pt. In the presence of Pt, we see an initial rise of $MV^{+\bullet}$, followed by a fractional decay to establish a steady state concentration in about 200 s. The steady state concentration of $MV^{+\bullet}$ in the presence of Pt is significantly lower than the one achieved in the absence of Pt. The steady state yield of $MV^{+\bullet}$ also decreases with increasing Pt concentration. These results support the argument made in the previous section that the Pt acts as an electron sink, scavenging electrons from the $MV^{+\bullet}$ radical.

Furthermore, when the light is turned off, the decay of the $MV^{+\bullet}$ is influenced by the presence of Pt. The $MV^{+\bullet}$ decays faster in presence of Pt, as the lifetime of the decay decreases from 602 s without Pt to 42 s at 0.5 μM Pt. In the absence of Pt, the recombination with residual holes in CdSe dictates the decay of $MV^{+\bullet}$. Since Pt acts as a mediator to accept electrons from $MV^{+\bullet}$ and discharge into the electrolyte (*e.g.*, re-

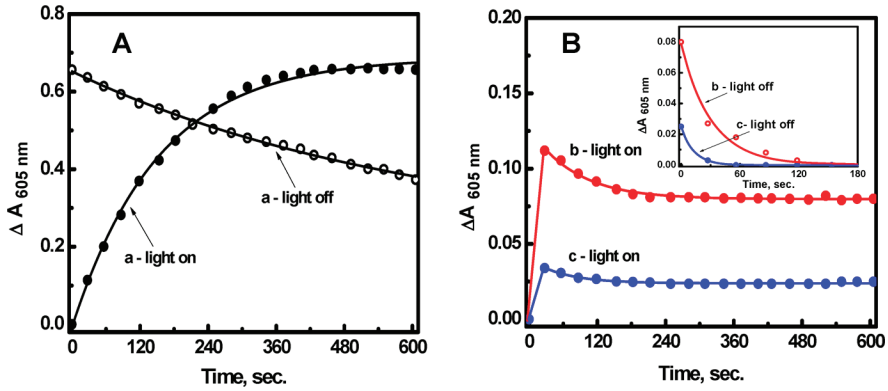


**Figure 5. (A)Accumulation of $MV^{+\bullet}$ during steady illumination (450 nm) of a solution of 1.38 μM CdSe and 1 mM $MV^{2+}$ in heptane/AOT/water reverse micelles (light on) and decay of the $MV^{+\bullet}$ radical upon stopping the illumination (light off). (B). Accumulation of the $MV^{+\bullet}$ following illumination of a reverse micelle solution of 1.38 μM CdSe and 1 mM $MV^{2+}$ containing (b) 0.5 μM Pt NP; (c) 1 μM Pt NP. The inset shows the decay of $MV^{+\bullet}$ after stopping the illumination**

duction of $H^+$), we observe a faster disappearance of $MV^{+\bullet}$. The stability of the $MV^{+\bullet}$ is also influenced by the ability of unbound radicals to escape from the parent micelle following electron exchange with bound $MV^{2+}$ molecules residing at the CdSe surface, which explains the long lifetime observed in Figure 5.

In previous experiments, the stabilization of free $MV^{+\bullet}$ radicals following excitation of CdSe was observed on the microsecond time scale using laser flash photolysis.[42] The conjunction of transient and steady-state absorption results confirm that the oxidation of the free $MV^{+\bullet}$ radicals by CdSe surface holes is a diffusion-controlled process. Similarly, diffusion controlled interaction between $MV^{+\bullet}$ and Pt particles has also been observed in earlier studies.[12−15]

Scheme 2 summarizes various charge transfer steps that dictate the accumulation of $MV^{+\bullet}$ in CdSe and CdSe−Pt systems. The rate constants determined from this study are also included. The initial excitation of CdSe leads to charge separation followed by charge recombination (reactions A and B). Both $MV^{2+}$ and Pt are good electron acceptors, as evident from the high values of the observed rate constants. In the absence of Pt, reactions E and F determine the net accumulation of $MV^{+\bullet}$. The relatively slow back electron transfer (reaction E) is due to the escape of $MV^{+\bullet}$ from the parent mi-

**Reaction Scheme and Measured Rate Constants**

| | | |
|---|---|---|
| $CdSe + hv \longrightarrow CdSe\,(e^-, h^+)$ | (A) | within pulse duration ($k_A > 8\times10^{12}\,s^{-1}$) |
| $CdSe\,(e^-, h^+) \longrightarrow CdSe$ | (B) | $k_B = 1.80 \pm 0.16 \times 10^9\,s^{-1}$ |
| $CdSe\,(e^-, h^+) + MV^{2+} \longrightarrow CdSe\,(h^+) + MV^{+\bullet}$ | (C) | $k_C = 1.7\times10^{10}\,s^{-1}$ |
| $CdSe\,(e^-, h^+) + Pt \longrightarrow Pt\,(e) + CdSe\,(h^+)$ | (D) | $k_D = 1.22\times10^9\,s^{-1}$ |
| $MV^{+\bullet} + CdSe\,(h^+) \longrightarrow CdSe$ | (E) | ps timescale for bound $MV^{+\bullet}$; diffusion-controlled process for free $MV^{+\bullet}$ (μs-sec timescale ) |
| $MV_a^{+\bullet} + MV_b^{2+} \leftrightarrow MV_a^{2+} + MV_b^{+\bullet}$ | (F) | $> k_H$ |
| $Pt(e) + MV^{2+} \longrightarrow MV^{+\bullet} + Pt$ | (G) | not observed |
| $MV^{+\bullet} + Pt \longrightarrow Pt\,(e) + MV^{2+}$ | (H) | $k_H \approx 3\times10^9\,s^{-1}$ |
| $Pt\,(e) + CdSe\,(h^+) \longrightarrow CdSe + Pt$ | (I) | - |
| $Pt\,(e) + H^+ \longrightarrow 1/2H_2 + Pt$ | (J) | - |

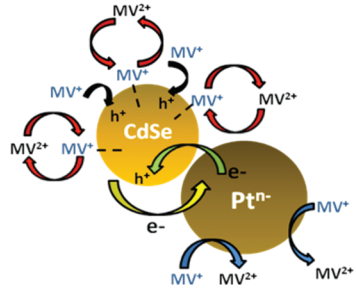


**Scheme 2. Reactions in a CdSe−Pt−$MV^{2+}$ coupled reverse micelle are shown. Dashed lines represent electrostatic interactions. Red arrows represent electron exchange mechanisms between free and surface bound methyl viologen ions. Blue arrows represent charge transfer between $MV^{+\bullet}$ and Pt. The green arrow shows oxidation of $Pt^{n-}$ by CdSe holes, while the yellow arrow shows direct electron transfer from CdSe to Pt. Black arrows show oxidation of $MV^{+\bullet}$ radicals by CdSe holes.**

celle (reaction F), which facilitates radical accumulation under steady state irradiation conditions.

The attainment of steady state accumulation of $MV^{+\bullet}$ is significantly affected when Pt nanoparticles are present. One would have expected a larger accumulation of $MV^{+\bullet}$ if Pt particles were directly mediating electron transfer to $MV^{2+}$ (reaction G). The low lying Fermi level of Pt makes it a good acceptor of electrons from photocatalytically generated $MV^{+\bullet}$ (reaction H). Both transient and steady state results show decay of $MV^{+\bullet}$ in the presence of Pt, thus indicating the dominance of reaction H over reaction G. The accumulation of $MV^{+\bullet}$ under steady state irradiation allows one to measure the equilibrium Fermi level of the semiconductor system.

Figure 5 shows the equilibrated absorbance values of accumulated $MV^{+\bullet}$ radicals following irradiation in the presence of CdSe, and CdSe/Pt ($\Delta A^{*}_{605} = 0.65$ for 1.38 μM CdSe; $\Delta A^{*}_{605} = 0.08$ for 1.38 μM CdSe + 0.5 μM Pt). Using Beer's law, the equilibrium concentrations of the $MV^{+\bullet}$ radical were calculated for both systems. By employing the Nernst equation, expression 7, we can obtain an apparent Fermi level ($E_F$) of the photocatalyst system.

$$E_F = E^0 + \frac{RT}{nF} \log \frac{[MV^{2+}]}{[MV^{+\bullet}]} \qquad (7)$$

By substituting the values of $[MV^{2+}]$, $[MV^{+\bullet}]$, and $E^0$ (−0.445 V *vs* NHE) we obtain the apparent Fermi levels of CdSe and CdSe/Pt as −0.366 and −0.312 V vs NHE, respectively. Although the difference between these apparent Fermi level potentials is small, it reflects the ability of Pt to (1) discharge electrons quickly, driving the Fermi level to a more positive potential, and, (2) to act as a microelectrode in the photocatalytic system. In contrast to Pt, studies with ZnO/Au and ZnO/Ag have shown a different scenario, in which gold/silver in contact with ZnO facilitates electron storage, driving the Fermi level to more negative potentials.[38] In the present study, the discharge of electrons mainly occurs through reaction with trapped holes at the CdSe surface (reaction I), or by reaction with $H^+$ to produce hydrogen (reaction J). The reduction of $H^+$ ions on the Pt surface in the $MV^{+\bullet}$/Pt system has been elucidated earlier using pulse radiolysis.[68] In the absence of a sacrificial electron donor, one would expect the back electron transfer to dominate. These important distinctions between the nature, size, and shape of cocatalyst metal nanoparticles need to be taken into account while designing photocatalyst assemblies.

## CONCLUSIONS

CdSe QDs and Pt nanoparticles are capable of interacting in a reverse micellar medium and undergoing an interactive coupling process. Electron transfer from excited CdSe to Pt occurs with a rate constant of $1.22 \pm 0.19 \times 10^9\ s^{-1}$ and an injection efficiency of 40%. When an electron acceptor, $MV^{2+}$, is introduced into the micellar medium, another pathway for deactivation of excited CdSe becomes apparent. The electron transfer, as monitored from the formation of the $MV^{+\bullet}$, is an ultrafast process. The rate constant of direct electron transfer from CdSe to $MV^{2+}$ is $1.7 \pm 0.11 \times 10^{10}\ s^{-1}$. In the presence of both $MV^{2+}$ and Pt, the CdSe bleaching recovery rate increases by an order of magnitude. The transient absorption spectra show that the photogenerated electrons are transferred to the surface-bound $MV^{2+}$ and then quickly scavenged by neighboring Pt particles, thus creating a channel for electron discharge. The electron equilibration between CdSe, Pt, and $MV^{+\bullet}$ thus plays a major role in dictating overall photocatalytic conversion efficiency. The lower accumulation of $MV^{+\bullet}$ in the CdSe−Pt system under steady-state irradiation is also indicative of the electrodic property of Pt nanoparticles as they discharge electrons both from CdSe and $MV^{+\bullet}$. The apparent Fermi level determined from steady state accumulation of $MV^{+\bullet}$ further highlights the important cocatalytic role that Pt plays in influencing the photocatalytic reaction. A mechanistic understanding of the reaction pathways and the kinetic details of individual reaction steps is important in the development of hybrid assemblies for solar fuel generation.

## EXPERIMENTAL SECTION

**Materials.** Reagent grade sodium sulfite (anhydrous) and dioctyl sulphosuccinate sodium salt (AOT) were purchased from Alfa Aesar. Selenium powder (200 mesh), methyl viologen, and anhydrous cadmium sulfate (99%) were purchased from Fisher Scientific and used as supplied. Chloroplatinic acid (99.9%) and hydrazine hydrate were purchased from Aldrich. Absorption spectra were recorded using a Cary 50 Bio UV−vis spectrophotometer. A 1 cm quartz cuvette was used.

**Femtosecond Transient Absorption Spectroscopy.** Ultrafast transient absorption measurements were conducted using a Clark-MXR 2010 laser system (387 nm, 1 mJ/pulse, fwhm 130 fs, 1 kHz repetition rate) and an Ultrafast Systems (Helios) detection system. The white light probe was generated by feeding 5% of the fundamental laser output (775 nm) through an optical delay line and focusing it on a quartz crystal. The optical delay provided a probe time window of 1.6 ns with a step resolution of 7 fs. The pump beam was attenuated at 5 μJ/pulse with a spot size of 2 mm (diameter) at the sample position where it was merged with the white light incident on the sample cell at an angle $< 10°$. After passing through the sample the probe beam was focused on a 200 μm core fiber connected to an Ocean Optics S2000 UV/vis CCD spectrograph (425−800 nm). Typically 1000 excitation pulses were averaged to obtain the transient spectrum at a set delay time. Kinetic traces at appropriate wavelengths were assembled from the time-resolved data. All measurements were conducted at room temperature by flowing deaerated sample through a 1 mm quartz flow cell.

**Steady State Photolysis.** The deaerated sample was excited in a 1 cm cuvette with collimated light from 250 W xenon lamp

passed through a 450 nm bandpass filter. A Ocean Optics S-2000 UV/vis CCD spectrograph was used to record absorption spectra in real time at preset time intervals during irradiation. CCD integration time was 300 ms and each data point was an average of 10 measurements.

**Synthesis of Pt Nanoparticles.** Two micelle solutions of equal water-to-surfactant ratio, $w_o$, containing the platinum salt and hydrazine precursors were prepared in separate vials and mixed. In one vial, 500 μL of 0.050 M $H_2PtCl_6$ was added to the 4.5 mL of 0.375 M AOT/heptanes. In the second vial, 500 μL of 0.1 M hydrazine was added to 4.5 mL of 0.375 M AOT in heptane. The resulting concentrations of AOT and $H_2O$ in the micelle solutions were 0.34 and 5.55 M, respectively ($w_o = 16.5$). This large value of $w_o$ was used to prevent the so-called "implosion mechanism", which is observed when the diameter of a Pt nanoparticle approaches the diameter of the encapsulating water pool. This results in surface capping of Pt by AOT molecules. Chen *et al*. demonstrated that the size of the Pt nanoparticles approaches a fixed value for $w_o > 10$ with low concentrations of $Pt^{4+}$.[44] To execute the synthesis of Pt nanoparticles, the two vials are mixed under vigorous stirring. The appearance of a deep brown color indicates formation of Pt nanoparticles. The particles are allowed to age for 24 h. The reaction is as follows:

$$H_2PtCl_6 + N_2H_4 \rightarrow Pt + 6HCl + N_2 \quad (8)$$

**Synthesis of Sodium Selenosulfate.** A stock solution of 0.10 M sodium selenosulfate, $Na_2SeSO_3$, was prepared by adding 0.395 g of Se powder and 1.26 g of $Na_2SO_3$ to 50 mL of distilled water. The slurry is then heated to 70 °C under vigorous stirring for 24 h. A clear solution is obtained.

**Synthesis of CdSe QDs.** Synthesis of CdSe followed the previously reported procedure in earlier work.[42] Two micelle solutions of equal $w_o$ containing cadmium and selenium precursors were prepared in separate vials and mixed. In one vial, 500 μL of 0.1 M $CdSO_4$ was added to 4.5 mL of 0.375 M AOT in heptane. The concentrations of AOT and $H_2O$ in the resulting micelle solution are 0.34 and 5.55 M, respectively ($w_o = 16.5$). In the second vial, to the same volume of heptane/AOT, was added 400 μL of 0.1 M $Na_2SeSO_3$ and 100 μL of distilled water. The separate micelle solutions must be sonicated until they become completely transparent, prior to mixing. The two solutions were then degassed and mixed under vigorous stirring (or sonication) to produce CdSe particles. An excess of $Cd^{2+}$ was used to ensure the neutralization of $Se^{2-}$ and to control the overall growth of particles. The particles are aged 24 h in a cool, dark location for complete growth. A bright orange solution is obtained as reaction 9 proceeds to completion.

$$Cd^{2+} + SeSO_3^{2-} + 2OH^- \rightarrow CdSe + SO_4^{2-} + H_2O \quad (9)$$

*Acknowledgment.* The research described herein was supported by the Department of Energy, Office of Basic Energy Sciences. We would like to thank Dr. Dan Meisel for helpful discussions. This is contribution number NDRL 4866 from the Notre Dame Radiation Laboratory.

*Supporting Information Available:* Results of Poisson analysis of the ionic and particulate contents of the micelles, transient absorption spectra, and kinetics of $MV^{+\bullet}$ formation. This material is available free of charge *via* the Internet at http://pubs.acs.org.

## REFERENCES AND NOTES

1. Henglein, A. Small-Particle Research: Physicochemical Properties of Extremely Small Colloidal Metal and Semiconductor Particles. *Chem. Rev.* **1989**, *89*, 1861–1873.
2. Henglein, A. Physicochemical Properties of Small Metal Particles in Solution: "Microelectrode" Reactions, Chemisorption, Composite Metal Particles, and the Atom-to-Metal Transition. *J. Phys. Chem.* **1993**, *97*, 5457–5471.
3. Kamat, P. V. Photophysical, Photochemical and Photocatalytic Aspects of Metal Nanoparticles. *J. Phys. Chem. B* **2002**, *106*, 7729–7744.
4. Kudo, A.; Miseki, Y. Heterogeneous Photocatalyst Materials for Water Splitting. *Chem. Soc. Rev.* **2009**, *38*, 253–278.
5. Matsumura, M.; Saho, Y.; Tsubomura, H. Photocatalytic Hydrogen Production from Solutions of Sulfite Using Platinized Cadmium Sulfide Powder. *J. Phys. Chem.* **1983**, *87*, 3807–3808.
6. Jin, Z.; Li, Q.; Zheng, X.; Xi, C.; Wang, C.; Zhang, H.; Feng, L.; Wang, H.; Chen, Z.; Jiang, Z. Surface Properties of Pt−CdS and Mechanism of Photocatalytic Dehydrogenation of Aqueous Alcohol. *J. Photochem. Photobiol., A* **1993**, *71*, 85–96.
7. Nosaka, Y.; Yamaguchi, K.; Kuwabara, A.; Miyama, H.; Baba, R.; Fujishima, A. Colloidal CdS−Pt Photocatalyst Stabilized by Pendant Viologen Polymer for Photoinduced Electron Transfer and Hydrogen Evolution. *J. Photochem. Photobiol., A* **1992**, *64*, 375–382.
8. Yoshimura, J.; Kudo, A.; Tanaka, A.; Domen, K.; Maruya, K.; Onishi, T. $H_2$ Evolution Caused by Electron Transfer Between Different Semiconductors under Visible Light Irradiation. *Chem. Phys. Lett.* **1988**, *147*, 401–404.
9. Parmon, V. N. Photoproduction of Hydrogen—An Overview of Modern Trends. *Adv. Hydrogen Energy* **1990**, *8*, 801–813.
10. Uchihara, T.; Abe, H.; Matsumura, M.; Tsubomura, H. Photocatalytic Hydrogen Evolution from Aqueous Solutions of Sodium Sulfite Using Platinum-Loaded $CdS_{1-x}Se_x$ Mixed Crystal Powder. *Bull. Chem. Soc. Jpn.* **1989**, *62*, 1042–1046.
11. Uchihara, T.; Matsumura, M.; Yamamoto, A.; Tsubomura, H. Effect of Platinum Loading on the Photocatalytic Activity and Luminescence of Cadmium Sulfide Powder. *J. Phys. Chem.* **1989**, *93*, 5870–5874.
12. Kiwi, J.; Graetzel, M. Protection, Size Factors, and Reaction Dynamics of Colloidal Redox Catalysts Mediating Light Induced Hydrogen Evolution from Water. *J. Am. Chem. Soc.* **1979**, *101*, 7214–7217.
13. Henglein, A.; Lindig, B.; Westerhausen, J. Photochemical Electron Storage on Colloidal Metals and Hydrogen Formation by Free Radicals. *J. Phys. Chem.* **1981**, *85*, 1627–1628.
14. Lee, P. C.; Matheson, M. S.; Meisel, D. Photogeneration of Hydrogen from Polymeric Viologen Systems. *Isr. J. Chem.* **1982**, *22*, 133–137.
15. Matheson, M. S.; Lee, P. C.; Meisel, D.; Pelizzetti, E. Kinetics of Hydrogen Production from Methyl Viologen Radicals on Colloidal Platinum. *J. Phys. Chem.* **1983**, *87*, 394–399.
16. Joshi, U. A.; Palasyuk, A.; Arney, D.; Maggard, P. A. Semiconducting Oxides to Facilitate the Conversion of Solar Energy to Chemical Fuels. *J. Phys. Chem. Lett.* **2010**, *1*, 2719–2726.
17. Maeda, K.; Domen, K. Photocatalytic Water Splitting: Recent Progress and Future Challenges. *J. Phys. Chem. Lett.* **2010**, *1*, 2655–2661.
18. Ng, Y. H.; Iwase, A.; Kudo, A.; Amal, R. Reducing Graphene Oxide on a Visible-Light $BiVO_4$ Photocatalyst for an Enhanced Photoelectrochemical Water Splitting. *J. Phys. Chem. Lett.* **2010**, *1*, 2607–2612.
19. Shankar, K.; Basham, J. I.; Allam, N. K.; Varghese, O. K.; Mor, G. K.; Feng, X.; Paulose, M.; Seabold, J. A.; Choi, K.-S.; Grimes, C. A. Recent Advances in the Use of $TiO_2$ Nanotube and Nanowire Arrays for Oxidative Photoelectrochemistry. *J. Phys. Chem. C* **2009**, *113*, 6327–6359.
20. Leng, W. H.; Barnes, P. R. F.; Juozapavicius, M.; O'Regan, B. C.; Durrant, J. R. Electron Diffusion Length in Mesoporous Nanocrystalline $TiO_2$ Photoelectrodes during Water Oxidation. *J. Phys. Chem. Lett.* **2010**, *1*, 967–972.
21. Licht, S.; Wang, B.; Ghosh, S.; Ayub, H.; Jiang, D.; Ganley, J. A New Solar Carbon Capture Process: Solar Thermal Electrochemical Photo (STEP) Carbon Capture. *J. Phys. Chem. Lett.* **2010**, *1*, 2363–2368.
22. Smotkin, E. S.; Cervera-March, S.; Bard, A. J.; Campion, A.; Fox, M. A.; Mallouk, T.; Webber, S. E.; White, J. M. Bipolar Cadmium Selenide/Cobalt(II) Sulfide Semiconductor

Photoelectrode Arrays for Unassisted Photolytic Water Splitting. *J. Phys. Chem.* **1987**, *91*, 6–8.
23. Frame, F. A.; Osterloh, F. E. CdSe-$MoS_2$: A Quantum Size-Confined Photocatalyst for Hydrogen Evolution from Water under Visible Light. *J. Phys. Chem. C* **2010**, *114*, 10628–10633.
24. Liu, L.; Hensel, J.; Fitzmorris, R. C.; Li, Y.; Zhang, J. Z. Preparation and Photoelectrochemical Properties of CdSe/$TiO_2$ Hybrid Mesoporous Structures. *J. Phys. Chem. Lett.* **2010**, *1*, 155–160.
25. Amirav, L.; Alivisatos, A. P. Photocatalytic Hydrogen Production with Tunable Nanorod Heterostructures. *J. Phys. Chem. Lett.* **2010**, *1*, 1051–1054.
26. Wang, C.; Thompson, R. L.; Baltrus, J.; Matranga, C. Visible Light Photoreduction of $CO_2$ Using CdSe/Pt/$TiO_2$ Heterostructured Catalysts. *J. Phys. Chem. Lett.* **2010**, *1*, 48–53.
27. Gopidas, K. R.; Bohorquez, M.; Kamat, P. V. Photoelectrochemistry in Semiconductor Particulate Systems. 16. Photophysical and Photochemical Aspects of Coupled Semiconductors. Charge-Transfer Processes in Colloidal CdS−$TiO_2$ and CdS−AgI Systems. *J. Phys. Chem.* **1990**, *94*, 6435–6440.
28. Fox, M. A.; Lindig, B.; Chen, C. C. Transients Generated Upon Photolysis of Colloidal $TiO_2$ in Acetonitrile Containing Organic Redox Couples. *J. Am. Chem. Soc.* **1982**, *104*, 5828–5829.
29. Arbour, C.; Sharma, D. K.; Langford, C. H. Electron Trapping in Colloidal $TiO_2$ Photocatalysts: 20 ps to 10 ns Kinetics. In *Photochemistry and Photophysics of Coordination Compounds*; Springer Verlag: Berlin, 1987.
30. Colombo, D. P. J.; Bowman, R. M. Femtosecond Diffuse Reflectance Spectroscopy of $TiO_2$ Powders. *J. Phys. Chem.* **1995**, *99*, 11752–11756.
31. Serpone, N.; Lawless, D.; Khairutdinov, R.; Pelizzetti, E. Subnanosecond Relaxation Dynamics in $TiO_2$ Colloidal Sols (Particle sizes $R_p = 1-13.4$ nm). Relevance to Heterogeneous Photocatalysis. *J. Phys. Chem.* **1995**, *99*, 16655–16661.
32. Colombo, D. P. J.; Rousal, K. A.; Saeh, J.; Skinner, D. E.; Bowman, R. M. Femtosecond Study of the Size-Dependent Charge Carrier Dynamics in ZnO Nanocluster Solutions. *Chem. Phys. Lett.* **1995**, *232*, 207–214.
33. Colombo, D. P. J.; Bowman, R. M. Does Interfacial Charge Transfer Compete with Charge Carrier Recombination? Femtosecond Diffuse Reflectance Investigation of $TiO_2$ Nanoparticles. *J. Phys. Chem.* **1996**, *100*, 18445–18449.
34. Furube, A.; Asahi, T.; Masuhara, H.; Yamashita, H.; Anpo, M. Femtosecond Diffuse Reflectance Spectroscopy on Some Standard $TiO_2$ Powder Catalysts. *Chem. Lett.* **1997**, 735–736.
35. Hodak, J. H.; Martini, I.; Hartland, G. H. Spectroscopy and Dynamics of Nanometer-Sized Noble Metal Particles. *J. Phys. Chem. B* **1998**, *102*, 6958–6967.
36. Sant, P. A.; Kamat, P. V. Interparticle Electron Transfer between Size-Quantized CdS and $TiO_2$ Semiconductor Nanoclusters. *Phys. Chem. Chem. Phys.* **2002**, *4*, 198–203.
37. Henglein, A.; Holzwarth, A.; Mulvaney, P. Fermi Level Equilibration Between Colloidal Lead and Silver Particles in Aqueous Solution. *J. Phys. Chem.* **1992**, *96*, 8700–8702.
38. Wood, A.; Giersig, M.; Mulvaney, P. Fermi Level Equilibration in Quantum Dot−Metal Nanojunctions. *J. Phys. Chem. B* **2001**, *105*, 8810–8815.
39. Subramanian, V.; Wolf, E. E.; Kamat, P. V. Green Emission to Probe Photoinduced Charging Events in ZnO−Au Nanoparticles. Charge Distribution and Fermi-Level Equilibration. *J. Phys. Chem. B* **2003**, *107*, 7479–7485.
40. Jakob, M.; Levanon, H.; Kamat, P. V. Charge Distribution between UV-Irradiated $TiO_2$ and Gold Nanoparticles. Determination of Shift in Fermi Level. *Nano Lett.* **2003**, *3*, 353–358.
41. Subramanian, V.; Wolf, E. E.; Kamat, P. V. Catalysis with $TiO_2$/Au Nanocomposites. Effect of Metal Particle Size on the Fermi Level Equilibration. *J. Am. Chem. Soc.* **2004**, *126*, 4943–4950.
42. Harris, C. T.; Kamat, P. V. Photocatalysis with CdSe Nanoparticles in Confined Media: Mapping Charge Transfer Events in the Subpicosecond to Second Timescales. *ACS Nano* **2009**, *3*, 682–690.
43. Uskokovic, V.; Drofenik, M. Reverse Micelles: Inert Nano-Reactors or Physicochemically Active Guides of the Capped Reactions. *Adv. Colloid Interface Sci.* **2007**, *133*, 23–34.
44. Chen, D. H.; Yeh, J. J.; Huang, T. C. Synthesis of Platinum Ultrafine Particles in AOT Reverse Micelles. *J. Colloid Interface Sci.* **1999**, *215*, 159–166.
45. Rivadulla, J. F.; Vergara, M. C.; Blanco, M. C.; Lopez Quintela, M. A.; Rivas, J. Optical Properties of Platinum Particles Synthesized in Microemulsions. *J. Phys. Chem. B* **1997**, *101*, 8997–9004.
46. Zhang, X.; Chan, K. Y. Water-in-Oil Microemulsion Synthesis of Platinum−Ruthenium Nanoparticles, Their Characterization and Electrocatalytic Properties. *Chem. Mater.* **2003**, *15*, 451–459.
47. Alkaitis, S. A.; Beck, G.; Graetzel, M. Laser Photoionization of Phenothiazine in Alcoholic and Aqueous Micellar Solution. Electron Transfer from Triplet States to Metal Ion Acceptors. *J. Am. Chem. Soc.* **1975**, *97*, 5723–5729.
48. Rafaeloff, R.; Tricot, Y. M.; Nome, F.; Fendler, J. H. Colloidal Catalyst Coated Semiconductors in Surfactant Vesicles. *In Situ* Generation of Rhodium-Coated Cadmium Sulfide Particles in Dioctadecyldimethylammonium Halide Surfactant Vesicles and Their Utilization in Photosensitized Charge Separation and Hydrogen Generation. *J. Phys. Chem.* **1985**, *89*, 533–537.
49. Lianos, P.; Thomas, J. K. Cadmium Sulfide of Small Dimensions Produced in Inverted Micelles. *Chem. Phys. Lett.* **1986**, *125*, 299–302.
50. Petit, C.; Jain, T. K.; Billoudet, F.; Pileni, M. P. Oil-in-Water Micellar Solution Used to Synthesize CdS Particles: Structural Study and Photoelectron Transfer Reaction. *Langmuir* **1994**, *10*, 4446–4450.
51. Petit, C.; Lixon, P.; Pileni, M. P. Synthesis of Cadmium Sulfide in situ in Reverse Micelles. 2. Influence of the Interface on the Growth of the Particles. *J. Phys. Chem.* **1990**, *94*, 1598–1603.
52. Pileni, M. P. Reverse Micelles as Microreactors. *J. Phys. Chem.* **1993**, *97*, 6961–6973.
53. Pileni, M. P.; Motte, L.; Jain, T. K.; Petit, C.; Billoudet, F., Synthesis and Photoelectrochemical Reactions of Cadmium Sulfide in Micellar Solutions. In *Electrochemistry in Colloids and Dispersions*; Mackay, R. A., Texter, J., Eds.; VCH Publishers: New York, 1992; p 375−383.
54. Pileni, M. P.; Motte, L.; Petit, C. Synthesis of Cadmium Sulfide *in Situ* in Reverse Micelles: Influence of the Preparation Modes on Size, Polydispersity, and Photochemical Reactions. *Chem. Mater.* **1992**, *4*, 338–345.
55. Nave, S.; Eastoe, J.; Heenan, R. K.; Steytler, D.; Grillo, I. What is so Special About Aerosol-OT? 2. Microemulsion Systems. *Langmuir* **2000**, *16*, 8741–8748.
56. Zulauf, M.; Eicke, H.-F. Inverted Micelles and Microemulsions in the Ternary System $H_2O$/Aerosol-OT/Isooctane as Studied by Photon Correlation Spectroscopy. *J. Phys. Chem.* **1979**, *83*, 480–486.
57. Atik, S. S.; Thomas, J. K. Transport of Photoproduced Ions in Water in Oil Microemulsions: Movement of Ions from One Waterpool to Another. *J. Am. Chem. Soc.* **1980**, *103*, 3543–3550.
58. Dimitrijevic, N. M.; Kamat, P. V. Transient Photobleaching of Small CdSe Colloids in Acetonitrile. Anodic Decomposition. *J. Phys. Chem.* **1987**, *91*, 2096–2099.
59. Brus, L. Quantum Crystallites and Nonlinear Optics. *Appl. Phys.* **1991**, *A53*, 465–474.
60. Burda, C.; Green, T. C.; Link, S.; El-Sayed, M. A. Electron Shuttling Across the Interface of CdSe Nanoparticles Monitored by Femtosecond Laser Spectroscopy. *J. Phys. Chem. B* **1999**, *103*, 1783–1788.
61. Wang, H.; deMelloDonega, C.; Meijerink, A.; Glasbeek, M.

Ultrafast Exciton Dynamics in CdSe Quantum Dots Studied from Bleaching Recovery and Fluorescence Transients. *J. Phys. Chem. B* **2006**, *110*, 733–737.
62. Dooley, C. J.; Dimitrov, S. D.; Fiebig, T. Ultrafast Electron Transfer Dynamics in CdSe/CdTe Donor−Acceptor Nanorods. *J. Phys. Chem. C* **2008**, *112*, 12074–12076.
63. Boulesbaa, A.; Huang, Z. Q.; Wu, D.; Lian, T. Q. Competition between Energy and Electron Transfer from CdSe QDs to Adsorbed Rhodamine B. *J. Phys. Chem. C* **2010**, *114*, 962–969.
64. Kongkanand, A.; Tvrdy, K.; Takechi, K.; Kuno, M. K.; Kamat, P. V. Quantum Dot Solar Cells. Tuning Photoresponse through Size and Shape Control of CdSe−$TiO_2$ Architecture. *J. Am. Chem. Soc.* **2008**, *130*, 4007–4015.
65. Robel, I.; Kuno, M.; Kamat, P. V. Size-Dependent Electron Injection from Excited CdSe Quantum Dots into $TiO_2$ Nanoparticles. *J. Am. Chem. Soc.* **2007**, *129*, 4136–4137.
66. James, D. R.; Liu, Y.-S.; de Mayo, P.; Ware, W. R. Distributions of Fluorescence Lifetimes: Consequences for the Photophysics of Molecules Adsorbed on Surfaces. *Chem. Phys. Lett.* **1985**, *120*, 460–465.
67. Lavalle, M.; Corda, U.; Fuochi, P. G.; Caminati, S.; Venturi, M.; Kovacs, A.; Baranyai, M.; Safrany, A.; Miller, A. Radiochromic Film Containing Methyl Viologen for Radiation Dosimetry. *Radiat. Phys. Chem.* **2007**, *76*, 1502–1506.
68. Brandeis, M.; Nahor, G. S.; Rabani, J. Reactions of Colloidal Platinum in Aqueous-Solutions Containing Methyl Viologen, Its Cation Radical, and Hydrogen, Studied by Pulse-Radiolysis. *J. Phys. Chem.* **1984**, *88*, 1615–1623.
69. Brown, J. M.; Bunton, C. A. Stereoselective Micelle-Promoted Ester Hydrolysis. *Chem. Commun.* **1974**, 969–971.
70. Duynstee, E. F. J.; Grunwald, E. Organic Reactions Occurring in or on Micelles. 1. Reaction Rate Studies of the Alkaline Fading of Triphenylmethane Dyes and Sulfonphthalein Indicators in the Presence of Detergent Salts. *J. Am. Chem. Soc.* **1959**, *81*, 4540–4542.
71. Duynstee, E. F. J.; Grunwald, E. Organic Reactions Occurring in or on Micelles. 2. Kinetic and Thermodynamic Analysis of the Alkaline Fading of Triphenylmethane Dyes in the Presence of Detergent Salts. *J. Am. Chem. Soc.* **1959**, *81*, 4542–4548.
72. Fisher, L. R.; Oakenfull, D. G. Micelles in Aqueous-Solution. *Chem. Soc. Rev.* **1977**, *6*, 25–42.
73. Kalyanasundaram, K. Photophysics of Molecules in Micelle-Forming Surfactant Solutions. *Chem. Soc. Rev.* **1978**, *7*, 453–472.
74. Mukerjee, P. Hydration of Micelles of Association Colloidal Electrolytes. *J. Colloid Sci.* **1964**, *19*, 722–728.